ARMA 17-686

Extension failure mechanisms explain failure initiation in deep tunnels *and* critical heights of cliff faces and near-vertical mountain walls

Barton, N.
Nick Barton & Associates, Oslo, Norway
Shen, B.
CSIRO Energy, Brisbane, Australia

Copyright 2017 ARMA, American Rock Mechanics Association

This paper was prepared for presentation at the 51st US Rock Mechanics / Geomechanics Symposium held in San Francisco, California, USA, 25-28 June 2017. This paper was selected for presentation at the symposium by an ARMA Technical Program Committee based on a technical and critical review of the paper by a minimum of two technical reviewers. The material, as presented, does not necessarily reflect any position of ARMA, its officers, or members. Electronic reproduction, distribution, or storage of any part of this paper for commercial purposes without the written consent of ARMA is prohibited. Permission to reproduce in print is restricted to an abstract of not more than 200 words; illustrations may not be copied. The abstract must contain conspicuous acknowledgement of where and by whom the paper was presented.

ABSTRACT: Brittle rock can fail due to extension strain over-coming the tensile limit, even when all stresses are compressive. Two related topics can thereby be addressed. The first is extension strain-induced failure in deep tunnels and mines, with fracture initiation in tension but subsequent propagation in shear. The familiar ratio of maximum tangential stress σ_θ / UCS of 0.4 ±0.1 signifying rock fracture initiation, and the initiation of acoustic emission, are each explained by the ratio of tensile and compressive strength and by Poisson's ratio, using a classic elastic equation and simple arithmetic. The maximum critical tangential stress σ_θ can actually be expressed as the ratio of tensile strength and Poisson's ratio σ_t/ν, hence the ratio 0.4±0.1. The second related topic is the *limited* heights of mountain walls, seen from the perspective of rock climbing. Limited in this case is a relative term: 1,000m to 1,350m of almost vertical meters challenge all rock climbers. This 'big-wall' range of heights is not exceeded anywhere in the world. Although strong granites are often involved, large-scale tensile strengths are apparently no larger than about 5 to 10MPa, due to weakening from temperature-cycling. At the other end of the spectrum, cliff houses in Cappadocia tuffs in Turkey may become exposed at intervals, due to extension failure of 15-20m high cliffs, with *in situ* tensile strengths of only 0.1MPa. Mountain heights limited to 8-9km can be explained by non-linear critical state rock mechanics: maximum shear strength is the limitation.

1. INTRODUCTION TO TUNNEL FRACTURES

Why do tunnels in massive rock start to exhibit fracture initiation when the ratio of the assumed maximum tangential stress σ_θ reaches approximately 0.4 x UCS? Why does acoustic emission in a laboratory compression test initiate at a similar ratio of principal stress and uniaxial compressive strength? Why do vertical cliffs in the ultra-weak Cappadocia tuffs in central Turkey tend to fail and expose underground dwellings or churches at intervals of a few decades or centuries, when their heights are even as little as 10 to 20 m? Why do the highest vertical mountain faces in the world of rock climbing range from 'no more' than 1,200 to 1,300m in height? Why did the first TBM tunnel in the world (1880) fail at its haunches when it curved beneath only a 70m high chalk cliff next to the Channel Tunnel, which was built 110 years later?

In the world of tunnelling we have come to expect *increased depth of break-out* when σ_θ /UCS > 0.4 (± 0.1), following a Canadian initiative (Martin et al. 1998). This is shown in Figure 1. Since 1993 we have used a rapidly accelerating value of the stress reduction factor SRF in the widely used single-shell Q-system tunnel-support recommendations, when σ_θ /UCS exceeds 0.4-0.5, as shown in Table 1. (Barton et al. 1974 showed SRF deliberately accelerated when the simpler ratio of σ_c/σ_1 reduced to below 5). Why do we need to reach a peak tangential stress of *only* 0.3-0.5 x UCS? Is this due to a scale effect, or due to an incorrect assumption?

Table 1. The 'accelerating' value of SRF when the ratio σ_θ/UCS ≥ 0.4, from the Grimstad and Barton, 1993 analysis of deep (600 to 1,400 m) road tunnels in Norway. Pre-1974 cases had suggested these limits: σ_c/σ_1 <5 or σ_t/σ_1< 0.33 required higher SRF and more robust tunnel support, reduced bolt c/c.

b) Competent rock, rock stress problems		σ_c/σ_1	σ_θ/σ_c	SRF
H	Low stress, near surface, open joints.	> 200	< 0.01	2.5
J	Medium stress, favourable stress condition.	200-10	0.01-0.3	1
K	High stress, very tight structure. Usually favourable to stability, may be unfavourable for wall stability.	10-5	0.3-0.4	0.5-2
L	Moderate slabbing after > 1 hour in **massive** rock.	5-3	0.5-0.65	5-50
M	Slabbing and rock burst after a few minutes in **massive** rock.	3-2	0.65-1	50-200
N	Heavy rock burst (strain-burst) and immediate dynamic deformations in **massive** rock.	< 2	> 1	200-400

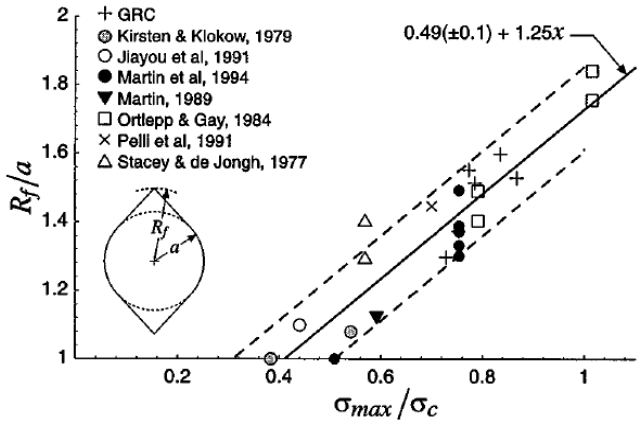

Figure 1. The method of interpreting (or predicting) depth of failure through 'over-stressing' (or over-straining, as just suggested) from Canadian and South African assemblies of data. After Martin et al., 1998.

The real answers to the '0.4±0.1 question' are very simple, but were not discovered until recently, when the second author was developing a new sub-routine for the DDM-based fracture mechanics code FRACOD, which is capable of modelling discrete tensile (extension) fracture initiation and propagation in shear, both in intact and jointed models of rock masses, using both mode I and mode II fracture toughness. The simple answers to the above questions do not require FRACOD discrete fracturing modelling, but simple arithmetic. However, this code will be used in several ways later in this paper.

When considering unjointed rock, a typical ratio of σ_c/σ_t is about 10, and a typical Poisson's ratio is about 0.25. It is shown in the Table 2 chain-of-logic that the *critical value of maximum tangential stress* σ_θ used in the much-used fracturing-threshold ratio of σ_θ/UCS = 0.4 (± 0.1) is in fact approximately equal to the ratio σ_t/ν, or tensile strength divided by Poisson's ratio.

A typical ratio of σ_t/ν for a strong granite might be 15/0.25 or 60 MPa. If UCS was 150 MPa, we would already see the reason for the threshold ratio of 0.4±0.1. To recap: 0.4±0.1 has been assumed to be the critical ratio of tangential stress/uniaxial strength, but the 'stress-induced' fracturing actually initiates as *extension-strain-induced* fracturing, due to exceedance of the critical extension strain in the radial (ε_3) direction. Stacey, 1981 can take most credit for the 'critical strain' concept. Martin et al.1998 give helpful descriptions too.

At higher stress levels or when a tunnel is deeper, fracture propagation is dominated by shearing, and this may resemble log-spiral surfaces as seen in polyaxial experiments when drilling under 3D stress.

A good example of 'stress' (or strain) induced fracturing was seen in five diversion and emergency spillway tunnels where they crossed the narrow ridge seen in Figure 2. Extremely high horizontal stresses were concentrated in this ridge. Fracturing occurred when the

Table 2. When developing a sub-routine for his fracture mechanics DDM-based code FRACOD, co-author Baotang Shen noticed the following logic, and ultra-simple arithmetic. Equations 1 (3D) and 2 (2D) were also used by Stacey, 1981.

$\varepsilon_3 = [\,\sigma_3 - \nu\,(\sigma_1 + \sigma_2)]\,/\,E$ (3D stress/strain)	$\varepsilon_3 = [\,\sigma_3 - \nu.\sigma_1]\,/E$ (2D stress/strain)

If $\nu\,(\sigma_1 + \sigma_2) > \sigma_3$, negative extension strain ($-\varepsilon_3$) occurs. In limit $-\varepsilon_{crit} = \sigma_t/E$	If $\nu.\sigma_1 > \sigma_3$ negative extension strain ($-\varepsilon_3$) occurs. If (-) $\varepsilon_3 > -\,\varepsilon_c$ (critical), then tensile failure occurs. Critical strain is given by: $-\varepsilon_{crit} = \sigma_t/E$

At tunnel wall, $\sigma_3 = 0$, and $\sigma_1 = \sigma_{\text{tang. critical}}$
Therefore (-) $\sigma_t/E = \varepsilon_c$ = (-) $(\nu.\sigma_{\text{tang. critical}})/E$

(Next: eliminate the common Young's modulus **E**)

$\sigma_{\text{tang. critical}} = \sigma_t/\nu \approx$	$\frac{UCS}{10\nu} = \frac{UCS}{10 \times 0.25} = 0.4 \times UCS$

tunnels passed through the most massive (Q > 100) basalt flows. In addition, tensile cracking was registered in all five inclined pressure tunnels, and in the spillway.

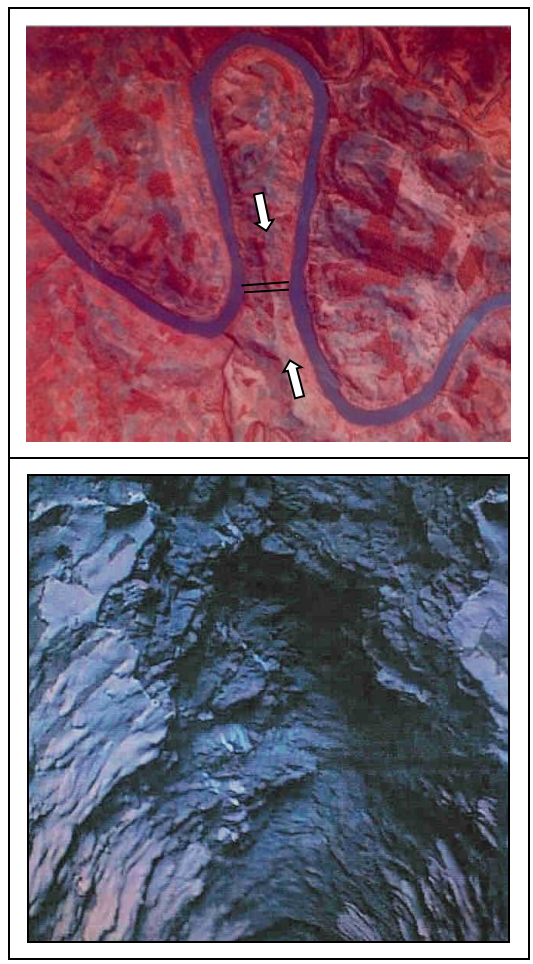

Figure 2. Site of Ita 1,400MW HEP, Brazil. Two to three meters of break-out, also in deepened inverts of five 14x16m tunnels, plus a basalt UCS = 200MPa, suggested via Figure 1 (due to σ_θ/UCS > 0.4), that k_0 (= σ_H/σ_v) could be in the extreme range of 20-25, due to the relatively shallow 75-125m depth of the tunnels. Barton and Infanti, 2004, Barton, 2010.

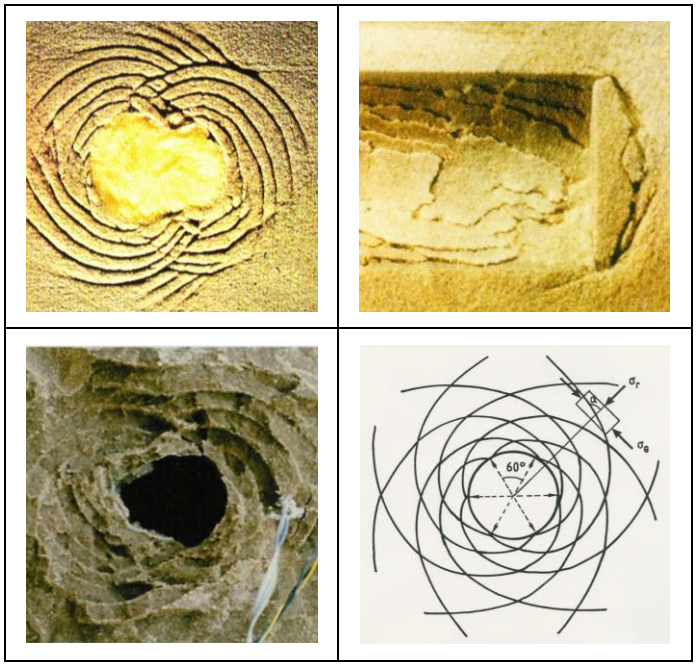

Figure 3. When principal stresses are even higher than UCS, as in these polyaxial drilling experiments to simulate deep well-bores in sandstone, then fracture propagation by log-spiral shearing is the dominant failure mode. Addis et al. 1990. (Classic log-spiral drawing from Bray, 1967).

2. PHYSICAL AND NUMERICAL MODELS

The best way to illustrate fracturing modes – is indeed by illustration, so this will be the trend in the remainder of this paper, especially when rock cliffs and big, nearly vertical walls of mountains are addressed.

Figure 3 shows what happens when the load-versus-strength is trending in the direction of one extreme: weak but brittle (cemented-sand) rock simulant loaded sufficiently to cause log-spiral shearing. These polyaxial 50 x 50 x 50 cm experiments, drilling into loaded sandstone blocks, were reported in Addis et al. 1990. We performed numerous such experiments and in all cases, due to the high loads, failure was through shearing, which was also recorded by miniature pre-drilled boreholes filled with coloured cemented sand – an idea from friend and former colleague Stavros Bandis †.

A good example of stress (or strain) induced failure from the real world, but still at the lower end of the strength scale, is shown in Figure 4. This and other tunnels in chalk marl, including the triple UK-France Channel Tunnels, were investigated together with John Sharp of Geo Engineering, in order to catalogue the prevalence of jointing and potential for over-break. (Barton and Warren, 1996). The 1880's Beamont TBM tunnel was driven through a curve in its early chainage, and over a length of just 150m, experienced wedge fall-out and then crushing (as in Figure 4) when 'suddenly' passing below a 70m high chalk cliff, possibly adding 2 or 3 MPa to σ_θ.

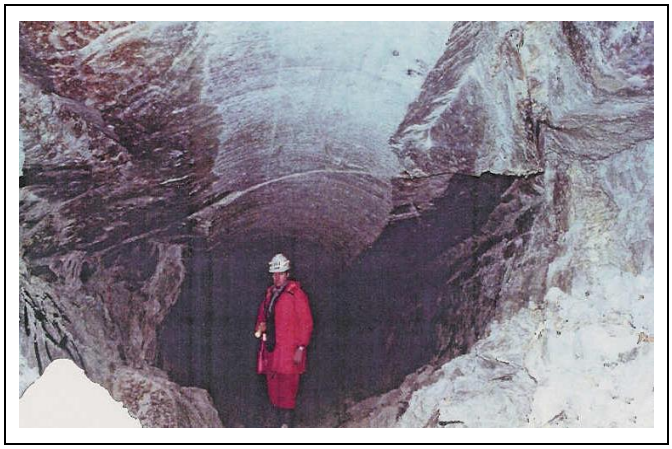

Figure 4. The 1880 Beaumont TBM tunnel which was a 110 years-too-early pilot tunnel for the 1990's Channel Tunnel between England and France. In this location, the weak but brittle chalk marl (UCS 4 to 9 MPa) was quite massive compared to its jointed, leaking nature (Q = 90/9 x ½ x 0.66/1) in some early sub-sea kilometers. Only bedding appears here.

A FRACOD model of this case is shown in Figure 5, and the assumptions for input data are listed in Table 3. In the progressive fracturing stages shown, the horizontal stress has been assumed to be one third of the vertical stress, apparently resulting in a quite realistic simulation. In Figure 6, by contrast, the horizontal stress is six times higher, showing what might occur in the arch and invert of an over-stressed (over-strained) tunnel in weak rock, if there was a 'tectonic-style' k_0 value of 2.0. As can be seen in both models, and right from the start, there is a combination of extension (tensile) fracturing (shown in red) with propagation in shear (shown in green).

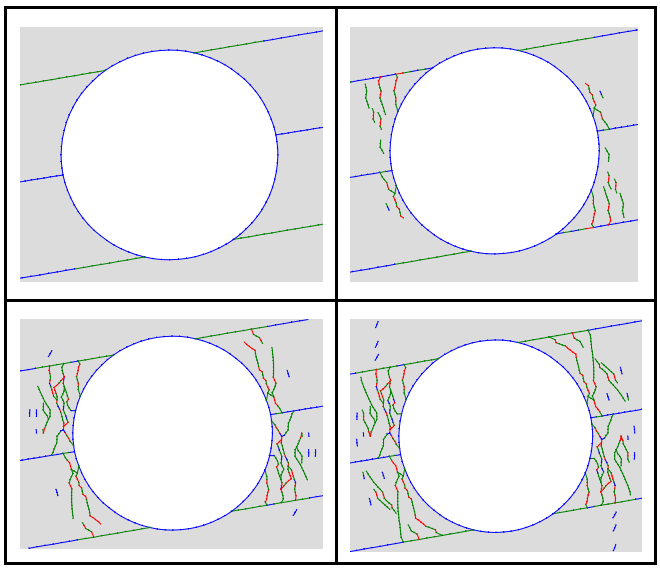

Figure 5. FRACOD models of the Beaumont tunnel fracturing, with input data given in Table 3. In this most realistic model $\sigma_H/\sigma_v = k_0 = 0.33$, which appears as a logical choice in view of the proximity of an adjacent cliff face and sloping shore line, the bedding planes are assumed, based on the single structure seen in the arch in Figure 4. (Note: red = tensile failure, green = shear failure).

Table 3. The input data that was assumed for the FRACOD models of chalk-marl shown in Figs. 5 and 6.

Property for FRACOD model	Value assumed
Young's modulus E	0.6GPa
Poisson's ratio ν	0.25
Density	2,000 kg/m^3
UCS	6MPa
Internal friction angle ϕ	30°
Cohesion c	1.73MPa
Tensile strength σ_t	0.173MPa
Fracture toughness K_{IC}	0.1MPa m$^{1/2}$
Fracture toughness K_{IIC}	0.2MPa m$^{1/2}$
Depth of cover	120 m
Vertical stress σ_v	2.4MPa
$\sigma_H/\sigma_v = k_0$	0.33, 2.0
Bedding plane dip, spacing	10°, 1 m
Bedding plane c and φ	0MPa, and 20°

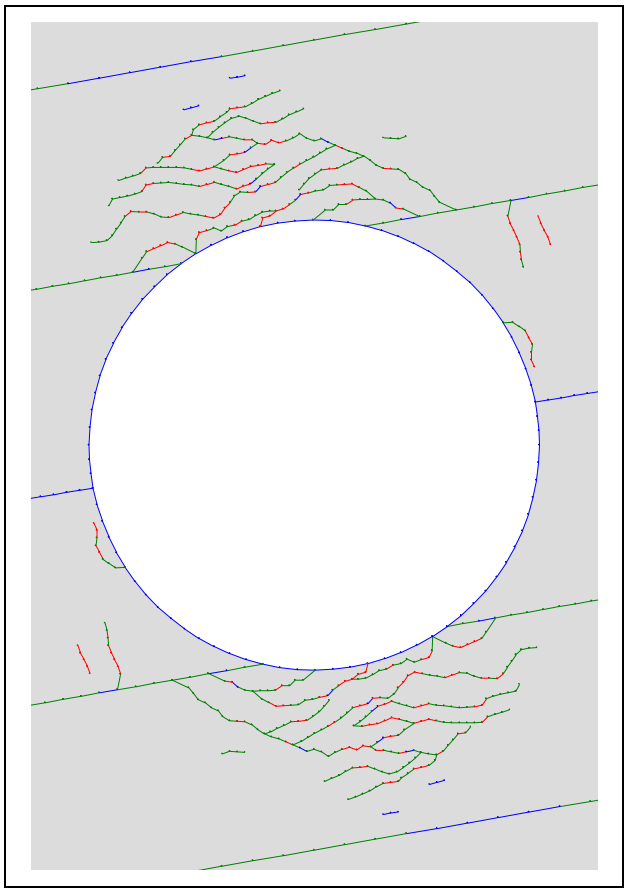

Figure 6. In this hypothetical case the horizontal stress is assumed to be dominant: $\sigma_H/\sigma_v = k_0 = 2.0$. The contrast to Figure 5 with $k_0 = 0.33$ is instructive. (Note: red represents tensile cracking, and green represents shear). Log-spiral tendencies are 'blocked' by bedding.

As we may observe in some of the mountain-wall photographs that follow later, thanks to the pioneering and fearless nature of our famous rock-climbers, there is also an indication of both modes of fracturing.

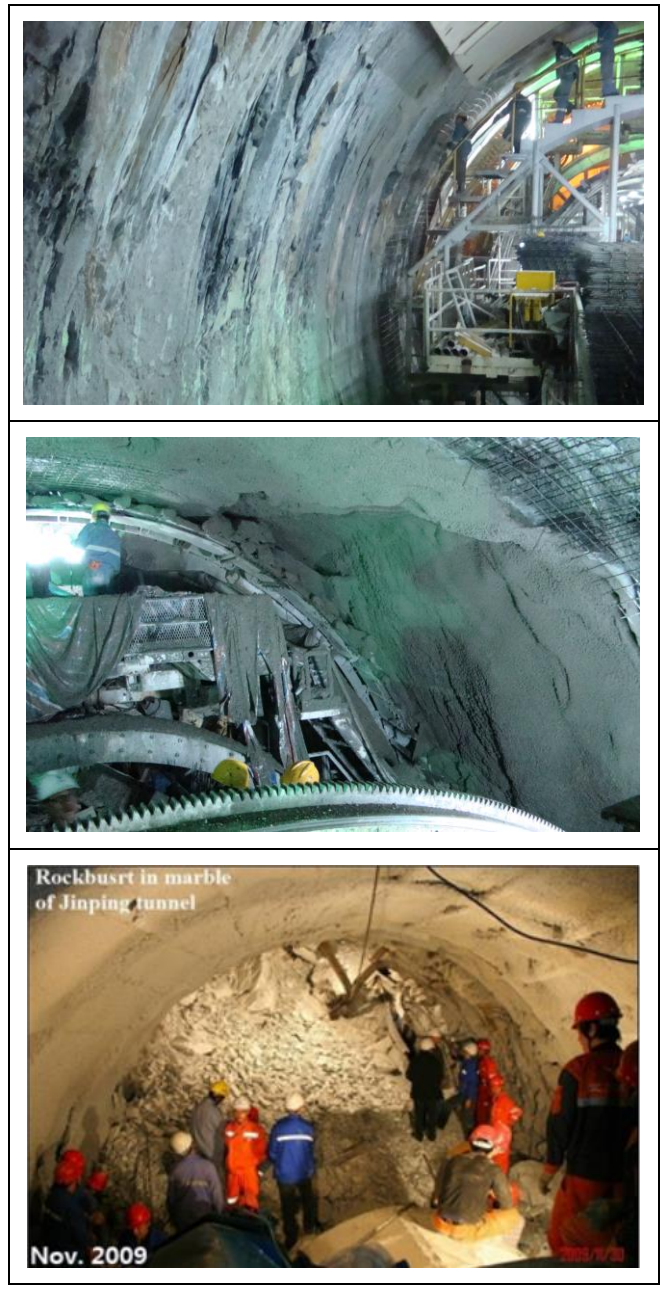

Figure 7. Three stages of TBM tunnelling in the Jinping I 16.7 km long headrace tunnels, under a mountain with several kilometers of almost 2.5km depth of cover. The marble, with UCS of mostly only 70 to 90 MPa was insufficiently strong in relation to maximum vertical stresses of at least 60-70MPa. Two of the four tunnels were initially driven by large-diameter TBM. (There was also a smaller pilot TBM). Eventually the three TBM had to be replaced by (also hazardous) drill-and-blast, following a big loss of life in the smaller pilot tunnel in November 2009. (Third photograph from 2016 conference in Hong Kong, concerning failure modes: www.igscsrm.hku.hk).

3. DEEP TUNNELS UNDER HIGH STRESS

Figure 7 illustrates 'three stages' of an optimistically designed major hydroelectric project in China (Jinping I). The top photograph illustrates what the first author interpreted as the tips of log-spiral shear failure surfaces.

This was one of the two large-diameter TBM at 'moderate' depth (in relation to the maximum 2,500m). Similar features were seen in the drill-and-blasted pair of parallel headrace tunnels. The second photograph was taken in the TBM tunnel with greater depth of cover, and it shows the effect of a moderate rock burst, caused by a major-principal vertical stress. Recommendations to proceed without the TBM could not be accepted, and regrettably the serious accident shown in the third photograph later occurred in the more advanced pilot TBM. This had even higher cover. Note the strong crushing of what was previously a (too) massive marble with insufficient (tensile and shear) strength.

In 2005, the first author had consulted on the almost equally deep (maximum approx. 2.0 km) Olmos water transfer project to be driven a remaining 14km through the Andes of northern Peru. It had been driven several kilometres from each end in an earlier Russian drill-and-blast contract. At this time, based partly on the results of Dr. Shen's contracted FRACOD models, two of which are shown in Figure 8, it was warned that drill-and-blast excavation would be preferable. This advice was due to the high 'theoretical' levels of tangential stress that tend to act (too) close to the periphery of smooth TBM tunnels, which are without the 'favourable' damage seen in the periphery of regular drill-and-blast tunnels.

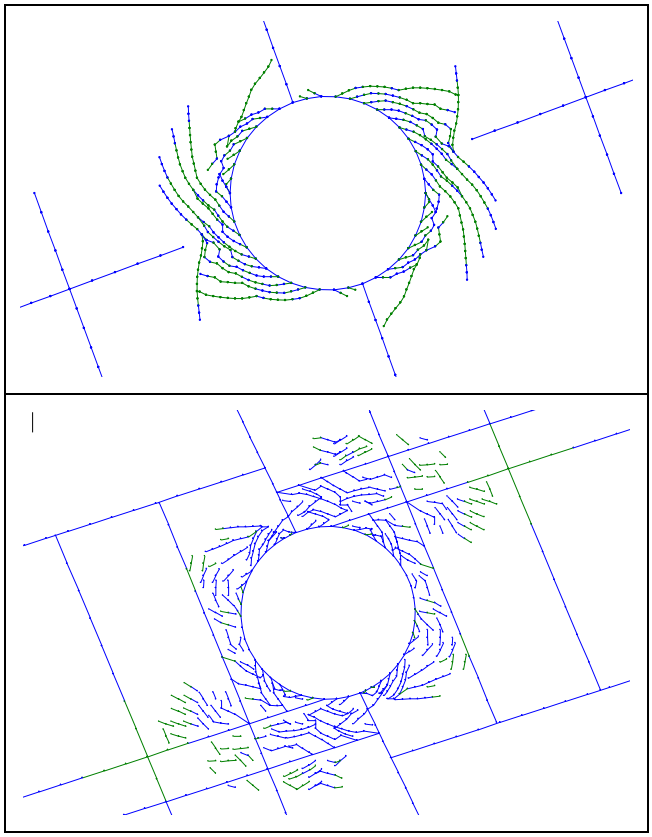

Figure 8 a and b. Exploratory FRACOD models, first with very limited jointing, then with some (axi-symmetric) jointing. The stress levels and properties had to be estimated, in view of the maximum 2km overburden and no available data. Top: σ_V = 55MPa, σ_h = 40MPa. Bottom: σ_v = 30MPa, σ_H = 60MPa.

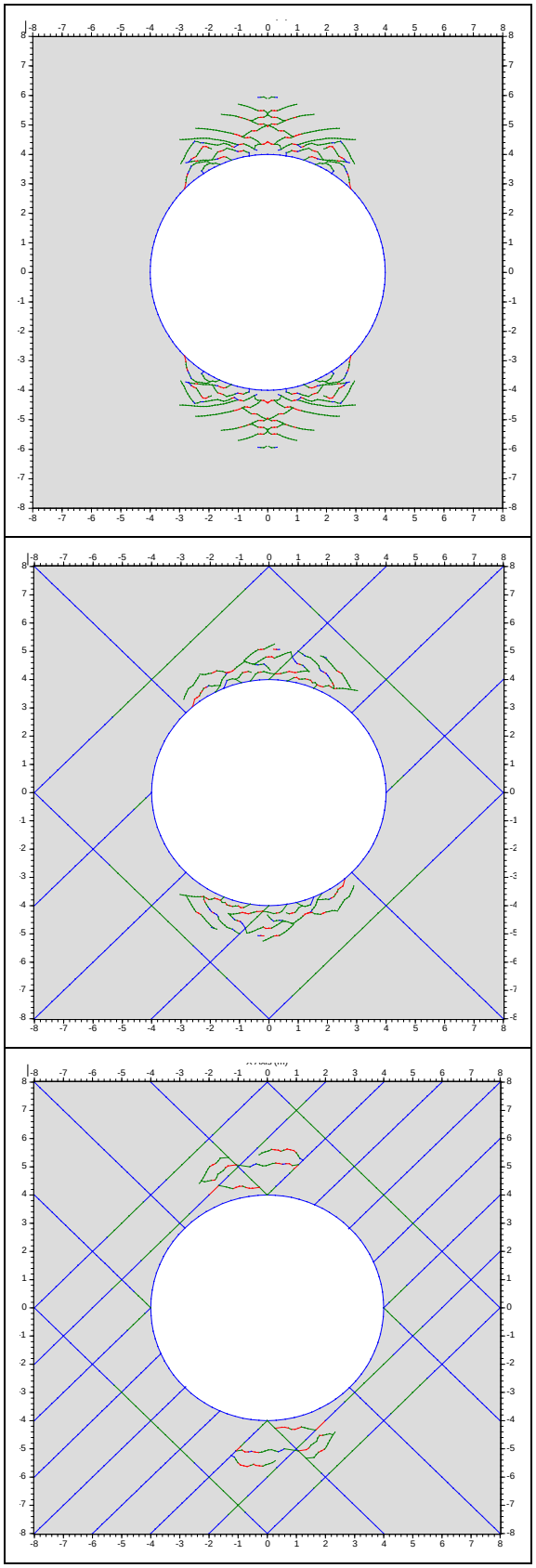

Figure 9. The potentially dissipating nature of jointing on the risk of rock-bursting due to dynamic shear fracturing was recently demonstrated by these and other models, in Barton and Shen, 2017. Displacement along any joints that are present helps to defuse the risk of unstable shear-fracture propagation. Jointing is seen to disturb/dissipate unstable log-spiral shearing, especially in the case shown in Figure 8.

In practice, the Olmos tunnel's remaining 14km of unexcavated ground had to be mostly excavated by TBM for contractual reasons. Several years of tunnelling problems and numerous rock bursts ahead of and above the cutter-head were experienced. The 'comminution' of the rock with numerous fine fractures (Figure 8b) appeared to be a realistic simulation of described conditions, with the benefit of hind-sight from the tough conditions described by Brazilian contractor Odebrecht. Sometimes circular steel sets were contorted into small local 'S-shapes by the energy of the dynamic loading.

The three more recent FRACOD modelling studies illustrated in Figure 9 have identical input data for the intact rock shown in Table 4. Each are simulating a tectonic-stress situation with k_0 = 2.0 and a depth of 1,000m. Note that the respective R_f /a ratios (refer to Figure 1) are approximately 1.5, 1.3 and 1.4, so apparent ratios of σ_θ/UCS are approximately 0.8, 0.6 and 0.7. The maximum tangential stress at the tunnel was calculated to be σ_{max} = 150MPa. Each of the above are realistic.

Table 4. The input data for the three FRACOD models shown in Figure 9 was the same as that reported for SKB's Äspö diorite, as reported in the literature and used for prior FRACOD models of the heated-pillar experiment (e.g. Siren, 2012 who compared Finnish and Swedish rocks from Äspö).

Property for FRACOD model	Value assumed
Young's modulus E	68GPa
Poisson's ratio ν	0.24
Density	2,500 kg/m^3
UCS	165MPa
Internal friction angle ϕ	49°
Cohesion c	31.0MPa
Tensile strength σ_t	14.8MPa
Fracture toughness K_{IC}	3.8MPa m$^{1/2}$
Fracture toughness K_{IIC}	4.7MPa m$^{1/2}$
Depth of cover	1,000m
Vertical stress σ_v	25MPa
$\sigma_H/\sigma_v = k_0$	2.0
Joint planes c and φ (M-C)	0.0MPa and 30°
Joint planes K_n and K_s	200 & 20GPa/m
Dilation angle φ_d	2°

The first half of this paper has dealt with stress (or strain) induced fracturing of the intact rock in massive or sparsely jointed rock masses, including both weak and strong rocks. Due of course to the rich geologic complexity of most rock masses, we have clearly addressed just a small portion of the many ways rock masses may respond to tunnel excavation. A more complete range of behaviour was suggested by Barton, 2003 (see Table 5). Some of this applies to rock slopes.

Table 5. Some of the rich selection of potential failure modes that may be observed in tunnels (and deep well-bores), depending on geology, strength and brittleness of the rock, and on the depths involved. Barton, 2003, Barton and Shen, 2017.

Description	Mode of behaviour
1. Hard, massive, brittle rocks that dilate during failure even when stresses are high. Stress-induced failure may be delayed as 'strength corrosion' occurs.	Extension failure, thin-walled stress-slabbing, dynamic ejection, bursting. The symmetric 'dog-eared' fall-out due to the aniso-tropic stresses may have a 'nose'. Deformations can be large.
2. Hard or medium hard, bedded and jointed rock that can shear and dilate along structural planes, while under moderate to high stress levels.	Anisotropic response. Shear stress dissipates by slight shear on bedding planes and joints. Deformations are moderate. Block falls can occur.
3. Soft, massive, non-brittle rocks that may, or may not dilate during shear failure. Typical for young e.g. Tertiary rocks such as the mudstones and siltstones in Japan.	Failure may occur by log-spiral shear development and tangential strain. Radial deformations are large, and pressure on support is high. (Twin tunnels need pillars 4 to 5 times their span c.f. Japan, Taiwan).
4. Very soft, plastic rocks (and clays) that contract when sheared under significant stress levels.	Post peak strength loss reaches an extreme of virtual "flow", tunnel closure can occur.

4. CLIFF HEIGHT-LIMIT FORMULATIONS

In a preliminary discussion of vertical cliffs, it will be convenient to refer to the following two diagrams which are borrowed from one of numerous recent soil mechanics texts, in this case following Verruijt, 2001.

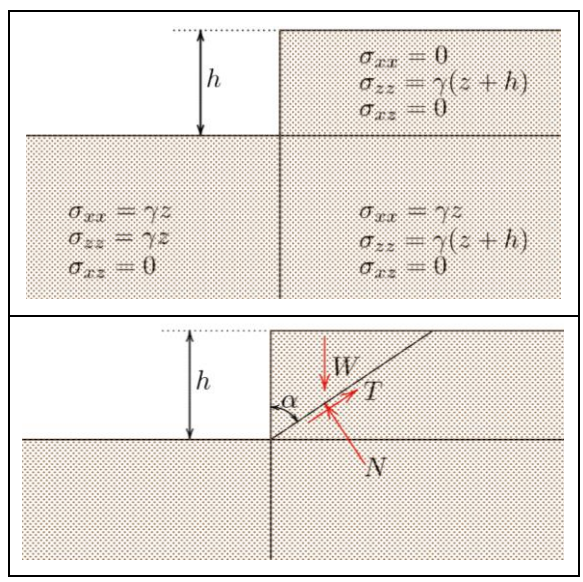

Figures 10 a and b. Several approaches to the stability of a vertical cut appear in soil mechanics literature. The assumed equilibrium of three zones in (a) gives a *lowerbound* solution.

First considering a purely cohesive material (with friction angle = 0°), and considering the equilibrium of the three distinct zones shown in Figure 10a, it can be shown that the *lowerbound critical cliff height* is:

$H_c = 2c/\gamma$ *(lowerbound, $\varphi = 0°$)* (3)

It is apparent that the 'exact' value of the multiplier can be increased to 2.82, 3.39 and even to 3.64 by utilizing ever more realistic assumptions for the actually somewhat complex stress distribution. (Verruijt, 2001).

The assumptions required for estimating the *upperbound critical cliff height* are illustrated in Figure 10b. In this case a single plane shear surface is assumed. Expressing the weight of the wedge as ½ $h^2 \tan \alpha$, it can be shown that the upperbound critical cliff height, again for a purely cohesive material ($\varphi = 0°$) is given when $\alpha = 45°$.

$H_c = 4c/\gamma$ *(upperbound, $\varphi = 0°$)* (4)

Using instead a circular slip surface as illustrated in Figure 11, Fellenius, 1927 reportedly derived a lower value for the *upperbound* multiplier of 3.83. So the highest *lowerbound* and the lowest *upperbound* are seen to have the following narrow limits (Verruijt, 2001).

$3.64c/\gamma \leq H_c \leq 3.83c/\gamma$ (5)

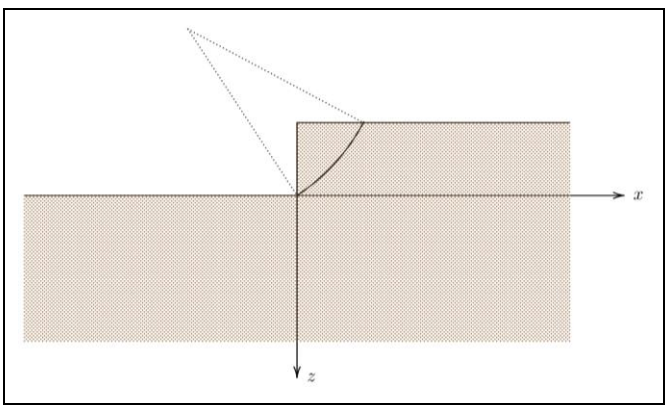

Figure 11. The circular failure surface assumption used by Fellenius, 1927 again for a frictionless material.

For the case of a *linear Coulomb material* with both cohesion and friction (c and φ), the *lowerbound* and *upperbound* solutions just given also include a friction angle, as in equation 6. Fellenius derived 3.85 for the multiplier, using a circular failure surface, and Drucker and Prager, 1952 suggested using a log-spiral failure surface for greater realism. *An exact solution is elusive:*

$2c/\gamma \tan(45° + \varphi/2) \leq H_c \leq 4c/\gamma \tan(45° + \varphi/2)$ (6)

In reality more complexity is involved in all of the above solutions because of various possible assumptions for stress distribution, and also because of strain and dilation dependent material behaviour. For the case of (almost)

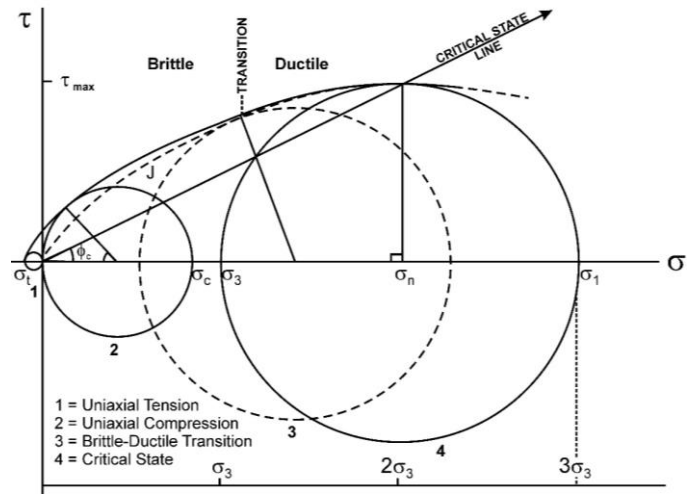

Figure 12. The strongly non-linear shear strength of intact rock and the *critical state concept* defining maximum possible shear strength. (Barton, 1976, 2013). (*Linear* Mohr-Coulomb does not apply over very large stress ranges). Note that Singh et al. 2011 confirmed that the values of σ_c and $\sigma_{3\ critical}$ are equal or nearly equal for the majority of rock types. We therefore have the significant situation that $\tau_{max} \approx \sigma_c$. This has repercussions for the unexpectedly simple equation suggested by Terzaghi, 1962, which can be shown *not working* for cliffs or steep mountain faces, but unexpectedly *'working'* for the maximum heights of the world's highest mountains. (Fourteen are between 8 and 9 km). The probable importance of the critical state for these maximum heights is discussed later.

intact rock, the medium of most interest from now on, we need to consider the strong non-linearity of the shear strength. Since *cliffs* can be 'stretched' to *mountain-wall* heights of 1 km or more, it is important to accept that both c and φ in equation 6 need to become stress-dependent variables. Figure 12 illustrates a promising scheme for the actual non-linearity, which was suggested a long time ago by Barton, 1976 following a wide review of high-pressure triaxial tests, mostly performed by Mogi and Byerlee. The critical state suggestion and the curvature has since been quantified by Singh et al., 2011 and more recently by Shen et al., 2017 (in press).

With reference to the figure caption for Figure 12, we now have to address the controversial Terzaghi, 1962 suggestion of a classically simple but *rather erroneous equation for the vertical height of rock cliffs*. Various authors have emphasized that his equation greatly exaggerates (by a factor of three to four) the possible heights of known rock cliffs. See examples on next page.

$H_c = q_c/\gamma$ (soil terminology), or $H_c = \sigma_c/\gamma$ (rock) (7)

We can conclude this brief review of 'cliff-height' equations, mostly from soil mechanics, by including the useful tension cut-off example shown in Figure 13. According to Chen and Scowthorn, 1968, the two methods of solution have coincident l*owerbound* and *upperbound* values of H_c for the tension-crack situation.

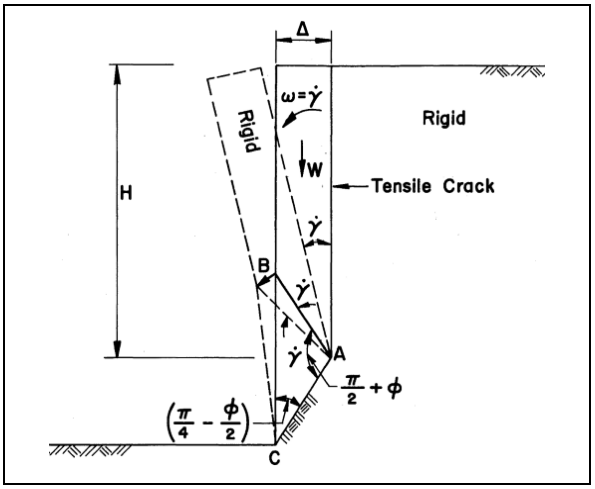

Figure 13. Coulomb strength with a no-tension cut-off, to allow for the effect of a tension crack, allows both the lower-bound and upper-bound solutions to coincide (Chen and Scowthorn, 1968).

The following formulation for H_c applies. (It is equal to the previous *lowerbound* solution for an 'intact' slope):

$$H_c = 2c/\gamma \tan(45° + \varphi/2) \quad (8)$$

Let us now consider the example of a moderately strong rock with UCS = 50 MPa. Terzaghi's Equation 7 predicts a maximum cliff height of 2,000m, if rock density was just 2,500kg/m^3, such as for a typical sandstone. Granite with even a moderately reduced *in situ* UCS of 100-150 MPa would suggest maximum vertical 'cliff heights' of 3,600-4,800m if a density of 2,750kg/m^3 was assumed. (Consistent units for this equation are kN/m^2 (e.g. 100 MPa x 1000) to convert to kN/m^2 and density kN/m^3 (e.g. 27kN/m^3 granite), with acceleration due to gravity 9.86 m/s^2 already accounted for). We know that such heights as 2.0, 3.6 and 4.8km are impossible for vertical or near-vertical mountain walls, and in the next section will show some of the world's highest known 'cliffs': which for instance are approximately 750m for sandstone, and approximately 1,250m for granite. The record may be 1,340m for the Great Trango Tower in the Karakoram mountain range in Pakistan. So an error of 3:1 or 6:1 is apparent, if trying to apply 'soil' solutions to a medium that is brittle, and therefore usually fails in a different manner.

However, when Terzaghi's equation 7 is applied to the maximum possible height of mountains, it may be 1:1 in apparent 'accuracy', but is not consistent with the critical state logic shown in Figure 12. It gives a reasonable result for the wrong reasons. Isostatic uplift ('floating' mountain chains), and the weakening effects of heating and pore-pressure are all big uncertainties of where the estimation of equilibrium should be made: a sub-mountain depth of 10 km as a round figure might be a starting point. With an assumed composite density of 2,850kg/m^3 and 8,500m of pore water pressure (both chosen for simplicity), a maximum rock 'compressive' strength of 200MPa seems to be needed. In fact the shear strength of 200 MPa is the weakest link, compared to a much too high $\sigma_{1\,max} \approx 3\ \sigma_{3\,crit} \approx 3$ x UCS = 600MPa.

Concerning the necessary evaluation of 'soil mechanics' formulations summarized in equation 6, we need to make appropriate estimates of cohesion. The same 'sandstone' and 'granite' examples can be used again. Referring to Figure 12 for convenience, a *lowerbound* estimate of cohesion (c) would be obtained most simply by assuming a straight-line, rather than the curved tangent between the uniaxial tension (σ_t) and uniaxial compression (σ_c) Mohr circles. The simple equation for this *lowerbound* (c), derived from Mohr circle geometry, was given in Barton, 1976:

$$c = ½\ (\sigma_c.\sigma_t)^{1/2} \quad (9)$$

If we examine the above formulations with the foregoing examples of a moderately strong sandstone valley-wall (UCS = 50 MPa) and a massive-scale mountain-wall in granite (conservative UCS = 100MPa) we can start by assuming that $\sigma_c/\sigma_t \approx 10$. (The range might be 5 to 20.)

1. Sandstone σ_c = 50MPa, σ_t = 5MPa
   c = ½(50x5) $^{1/2}$ = 7.9MPa
2. Granite σ_c = 100MPa, σ_t = 10MPa
   c = ½(100x10) $^{1/2}$ = 15.8MPa

The gradient of the presently assumed straight line between the tensile and compressive strength Mohr circles, giving a *lowerbound* value of c is given by:

$$\sigma_c/\sigma_t = \tan^2(45° + \varphi/2) \quad (10)$$

A common friction angle φ of approximately 56° is indicated if σ_c/σ_t=10. Using just the *lowerbound* solution given by equation 6, serious errors are evident.

Sandstone cliff $H_c = 2c/\gamma \tan(45°+\varphi/2)$
H_c=2x7.9x1000/25 tan (45° + 28°) = 2,067m

Granite mountain-wall
H_c=2x15.8x1000/27.5 tan (45°+ 28°) = 3,759m

(Using the 'soil mechanics' *upperbound:* the right-hand side of equation 6, these 3:1 errors are doubled). Except for the case of huge rock avalanches (Figure 15c) seldom experienced in recorded history, it is clear that even this *lowerbound* solution, borrowed from soil mechanics and based on *shear strength*, cannot be applied to vertical rock cliffs. So we remain in urgent need of a 'cliff formula' for brittle rock. Our solution is to combine *Poisson's ratio (ν) and tensile strength (σ_t)*, from the 'tunnel-failure logic' of Table 1, with the assumed *maximum vertical stress (γH/100)* in MPa. Note that *ν* is an irresistible component of elasticity. *Geomorphology meaning the slow degradation of too high or too steep mountains, usually will select the weakest link (σ_t) for preferential failure, seldom 'choosing' c or σ_c of rock.*

5. THE OBSERVATIONAL METHOD

Due to their pioneering drive and (almost) fearless skills, mountain-wall and Alpine-style climbers have been conquering the highest and steepest mountains and mountain walls for the last sixty years. Many first ascent

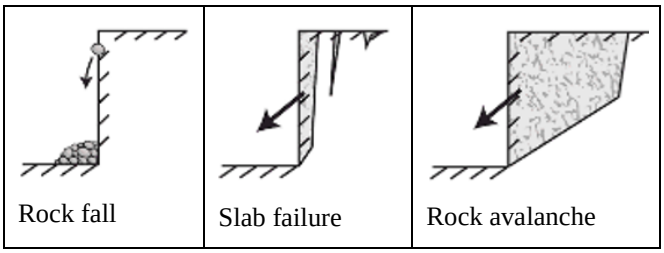

Figure 14. Three of the principal cliff (or mountain-wall) degradation and failure processes, as envisaged by Melosh, 2011. These have been presented in this figure in the order of frequency-of-occurrence, using just three of his categories.

records of the highest mountains in the 1950's, and more and more competitive and free-solo wall-climbing in the last twenty years has meant that the internet is generously supplied with hundreds of thousands of photographs. As 'desk-bound' researchers in relation to these daring climbers (and climbing photographers), the liberty has been taken to re-size (to square format) the most illustrative cases, to aid in our exploration of fracturing processes caused by extensional strain, exceedance of tensile strength, and propagation in shear.

In popular tourist areas and renouned rock-climbing meccas, like the Yosemite National Park in eastern California ('the valley' to American rock climbers), detailed records of the thousands of rock falls and occasional slab failures have been kept by the Park service, assisted by the USGS and others. Stock et al., 2012 contains a remarkable documentation of the first two categories shown in Figure 14, from Melosh, 2011.

Fortunately the third category, the *rock avalanche* is a seldom, though devastating occurrence, with velocities and travel distances that defy understanding, unless one invokes instantaneous steam formation due to the heat-generated transformation of ground-water to load-bearing steam. A case known to the writers (Marte Gutierrez, priv. comm.) saw rescue workers unable at first to dig down to a buried town in the Phillipines, due to the high temperature of the rock and mud debris.

Before reproducing photographs of mountain walls, Figure 15 may be helpful to visualize vertical stress distributions, using finite element analyses of a theoretical (less common) vertical cliff, and of a more typical, *almost-vertical* situation. The latter corresponds well to the extreme mountain walls to be illustrated. Note the different sizes of the theoretical (isotropic, elastic, continuum) tension zones at the top of the 'cliffs'. These zones are adverse areas for the initiation

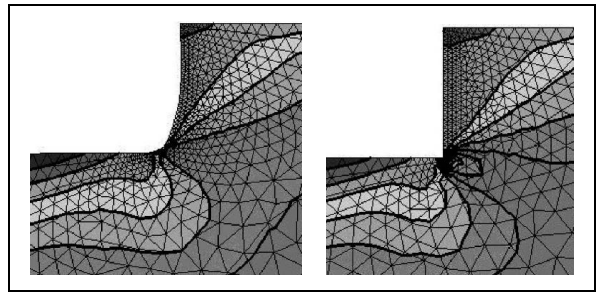

Figure 15. FEM models of principle (vertical) stress for vertical and semi-vertical cliffs given by Wolters and Müller, 2008. Their studies also showed that if a tension crack is modelled, 'a line' of high shear stress will tend to develop from the base of the crack to the highly-stressed (and strained) toe of the slope, showing similarity to Figure 13 in fact.

of degradation by tension crack formation, aided by water pressure, ice-wedging, internal block-wedging, and the constantly fluctuating temperature which is known to weaken all rocks. An excellent recent article on the subject from the Matterhorn is Weber et al. 2016.

Four of the very highest almost vertical mountain walls known to the world's climbing profession are illustrated on the next page. They are awe-inspiring to both layman and expert climber. They provide an interesting contrast to mountains which appear to show (prior) shear failure, or the effect of major joint sets (refer to Figure 16), where possibly lower shear strengths have allowed such failure surfaces to develop in preference to the *slab-failures* that can be assumed to have dominated in the gradual mountain degradation that we see in the high walls formed of the strongest brittle rocks.

Figure 16. Presumed historic shear failures, or the influence of prior geologic structure, in weaker rocks. Selected from the Karakoram, Pakistan. Prior anisotropic stress is suggested.

Cerro Torre, Patagonia, Chile: 1,230m

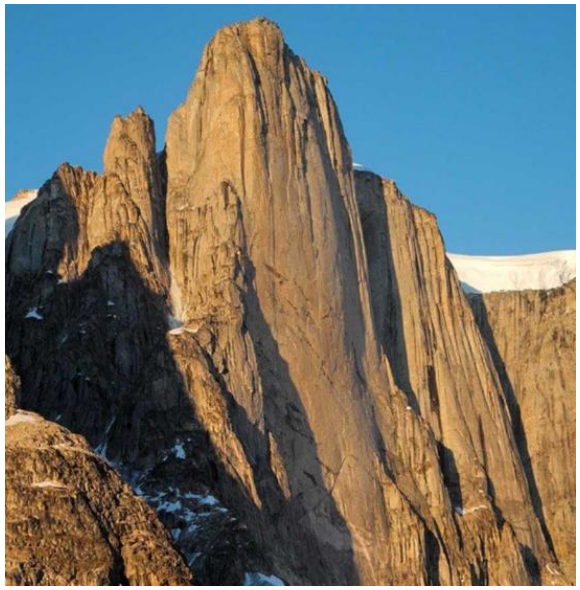

Mirror Wall, Greenland: 1,200m

Figure 17 a and b. Cerro Torre, Patagonia, and Mirror Wall, Greenland with near-vertical heights of approx. 1,230m and 1,200m

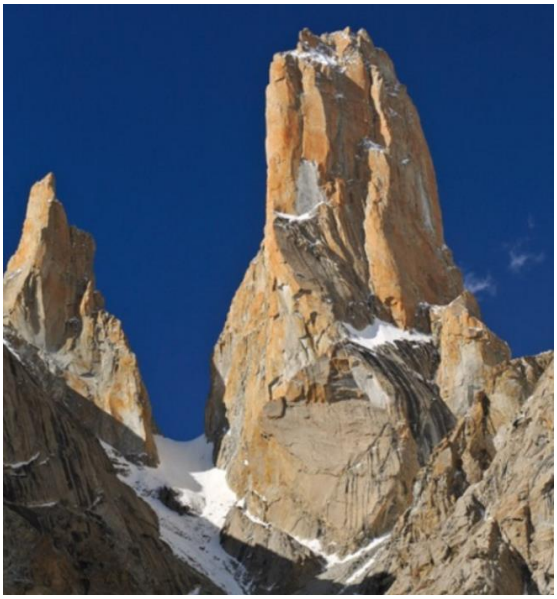

Great Trango Tower, Karakoram, Pakistan: 1,340m

Mount Thor, Baffin Island, Canada: 1,250m

Figure 17 c and d. Great Trango Tower, Karakoram and Mount Thor, Baffin Island, generally considered to be the world's two highest near-vertical mountain walls.

6. NEW CLIFF-HEIGHT FORMULA FOR ROCK

The foregoing review of classical soil-based equations has revealed (confirmed) the inadequacy of these when applied to failure of intact rock. The reasons can be easily explained. A trench failure or a cut-slope failure due to inadequate sheet-piling or soil-nailing, might involve 5, 10 or at worst 15m of failed excavation in the soil. For intact rock to fail in the (shear failure) manner of soils (equations 3, 4, 5 and 6), huge cohesive strength has to be overcome, perhaps as much as 5,000 to 25,000 kPa (5 to 25 MPa). One is immediately at mountain-scale if the necessary tens of MPa shear stresses should be generated. Alternatively, as immediately concluded by Terzaghi, 1962, the rock has actually to be a *jointed rock* mass with sufficient planes of weakness. This is not disputed, but here we are examining how to explain the failure (or critical slope height) of massive, sparsely or unjointed rock, such as illustrated in Figures 17 and 18.

A rock avalanche with 500m vertical frontal height might travel more than 10-20km at speeds of hundreds of km/hr, if not hindered by an opposing mountain wall. It would be a major terrestrial event, incomparable with a deep trench failure in soil. Due to these short-comings

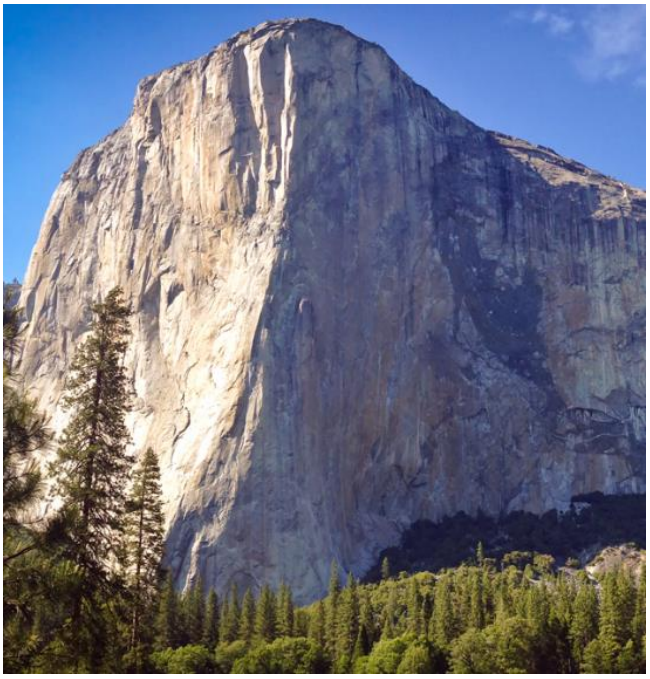

El Capitain, Yosemite, California, near-vertical granite: 1,000m (The Nose: Centre, Dawn Wall: right-of-centre). Estimated UCS = 100 to 150MPa.

Beachy Head, England, bedded chalk, 100m. Despite crossing numerous bedding planes, note relative planarity of extension fracturing. Estimated UCS = 25MPa

West Temple, Zion NP, Utah. sandstone, 670m. Claimed as the probable highest sandstone cliffs in the world. Estimated UCS = 75MPa.

Figure 18 a and b.

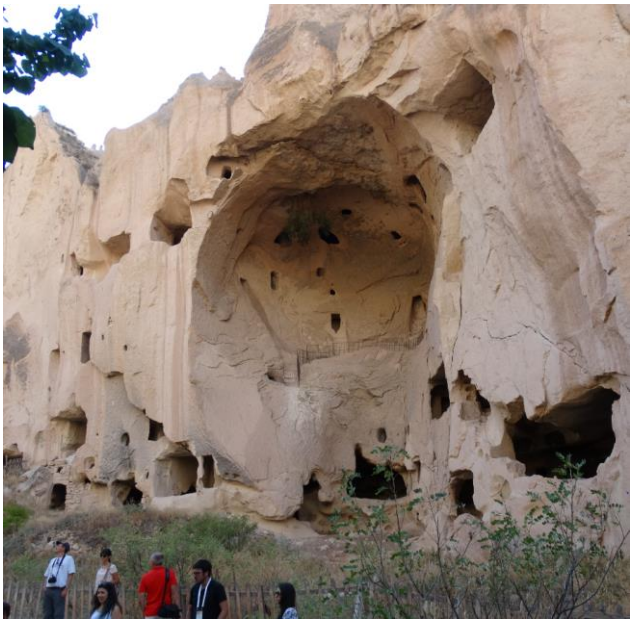

Ancient Christian dwellings and churches in Cappadocia region of Turkey, exposed here by historic, and more recent, 15m high cliff failure. Estimated UCS = 1 to 2MPa.

Figure 18 c and d.

and fundamental differences, an alternative equation is presented on the next page, based simply on equating the *critical tangential (or principal) stress* that will cause extensional failure (even in a compressive stress field) with the assumed vertical stress generated by the density and the height of the cliff in question.

As we have seen in the first half of this paper, extensional failure is governed by the ratio of σ_t/ν (tensile strength/Poisson's ratio). We simply equate this with the gravitationally generated assumed maximum vertical stress = $\gamma H_c/100$. Concerning maximum vertical cliff heights, over a wide range of rock strengths, we

find that the approximation:

$$H_c \approx (100.\sigma_t) / \gamma\ \nu \qquad (10)$$

involving tensile strength (σ_t), density (γ) and Poisson's ratio (ν), gives a much more accurate limiting height for vertical cliffs or mountain walls than the classic Coulomb, Terzaghi or soil mechanics based relationships that we reviewed earlier. This formulation, used in Barton, 2016 to explain both high mountain walls in granite, and limited cliff height failures in Turkey's Cappadocia tuffs, is a very simple extension of the second author's discovery of the reasons for the '0.4' ratio in tunneling (see Table 2 train-of-logic). Note that with σ_t expressed in tons/m^2 and density in tons/m^3, we get tons/m2/tons/m3 = m. We therefore have discovered an ultra-simple but *geomorphologically* effective equation, thanks to elastic theory and fracture mechanics

$$H_c = \sigma_t / \gamma\ \nu \qquad (11)$$

Cliff height failures of only 10 to 20m in the tuffs of Cappadocia, with UCS = 1 to 2MPa, or the 1,200m-1,300m mountain walls in 100-150MPa granites, are thereby more or less explained. A set of examples with progressively reduced strength and wall heights, are given in Table 5. The limiting value here is the *in situ* scale effect on the tensile strength, already the minimum strength component, but undoubtedly reduced slowly with time, until a slabbing fracture can form. There was a recent slab-failure in Yosemite Valley weighing several thousand tons, and measuring approx. 30 x 60 x 0.65m. When such a slab weakens, it accentuates the effect of temperature and moisture (and ice-wedging cycles) for the next layer of rock. In Figure 18, four distinctly different wall-heights and geologies were selected, in order to introduce the new ability to describe critical cliff heights for widely varying rock strengths.

Dramatic photographs of rock-climbing indicate that slab failures are what give the mountain face its (local) smoothness. Furthermore, the essential vertical crack paths loved (and needed) by climbers, that can run hundreds of meters up some classic climbing routes, are very likely to be an expression of the same extensional strain mechanism acting in the third (along the wall) direction. Thermal stress due to temperature change adds to the high vertical stress, and therefore elevates the extensional strain, also causing increased slabbing. A huge industry of nuts and bolts and exotic expanders are designed to allow rock climbers to progress up vertical cracks of varying width. Concerning using these cracks, the record for 'The Nose' route up the 1,000m of El Capitan in the Yosemite Park is now 2 hours and 23 minutes. Hans Florin, who has more than 160 ascents up The Nose was partnered by the world's foremost free-soloist Alex Honnold. The first ascent decades before took 45 days, spread over 18 months. (see Florin and Moye, 2016 Honnold and Roberts, 2016). Their recent books make for very exciting reading, especially for rock mechanics readers interested in especially long extension cracks. These books give excellent 'rock mechanics' insight, as seen through the eyes of arguably the world's two most famous rock speed-climbers since the sport began in the 1990's.

Table 5. Application of the new *rock-wall* equation 10, to a range of possible (intact) rock types. Some minor weakening of the tensile strengths has been undertaken, which is believed to be in line with the known or probable effect of temperature cycling (both daily and yearly). $H_c \approx (100.\sigma_t) / \gamma\ \nu$.

UCS 125MPa Hard rock	UCS 50MPa Medium hard rock	UCS 15MPa Low strength rock	UCS 2MPa Very low strength rock
$\sigma_t \approx 9$ MPa	$\sigma_t \approx 4$ MPa	$\sigma_t \approx 1$ MPa	$\sigma_t \approx 0.1$ MPa
$\nu = 0.25$	$\nu = 0.20$	$\nu = 0.15$	$\nu = 0.15$
$\sigma_t / \nu = 36$ MPa	$\sigma_t / \nu = 20$ MPa	$\sigma_t / \nu = 6.7$ MPa	$\sigma_t / \nu = 0.67$ MPa
$\gamma = 2.75$ tons/m^3	$\gamma = 2.5$ tons/m^3	$\gamma = 2.25$ tons/m^3	$\gamma = 2.0$ tons/m^3
$H_{crit} = 1309$m	$H_{crit} = 800$ m	$H_{crit} = 296$ m	$H_{crit} = 33$ m

7. MOUNTAIN-DEGRADATION PROCESSES

It is probably a 'sad reality', though not exactly a problem for this or the next many generations (of rock climbers) that the most impressive rock walls tend to be impressive because of their over-steepened state. This is because the proposed *σ_t / $\gamma.\nu$ mechanism of extension failure* has the effect of steepening and degrading mountain faces. An important initial steepening process may be the formation of cirques by active glaciers. One is illustrated in Figure 19. The extension/slabbing mechanism greatly assists the rate of glacial steepening.

Figure 19. Example of a glacially eroded cirque, and over-steepened head-wall. Baffin Island, NE Canada.

Relentless exfoliation due to temperature cycling, ice wedging and even the effect of relentless high winds. Close to Fitz Roy peaks, Patagonia, Chile.

An illustration of the role of variable geology on the 'longevity' of mountains. Note the slope debris from the hillside formed in layers of volcanic rocks. Cerro Torre is in the immediate background, Patagonia, Chile.

Figure 20 a and b.

Extensional strain, then ice-wedging and block-fall wedging emphasizes the impermanence of mountains, and the top of Cerro Torre in particular. Patagonia, Chile.

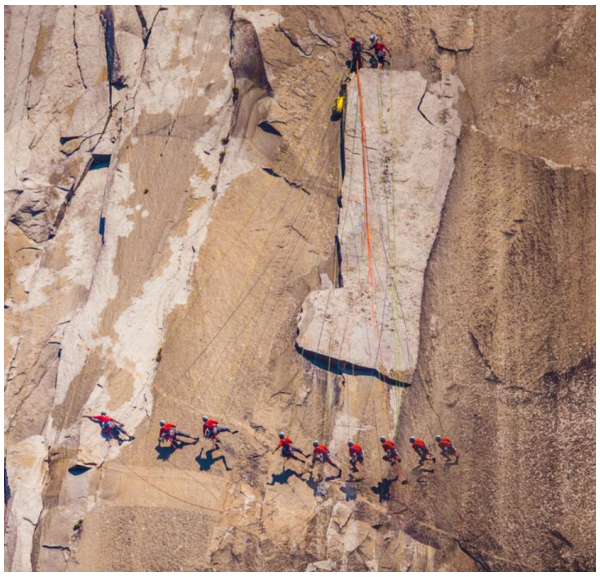

Hans Florine, known as 'Hollywood Hans' to his friends, is shown with time-laps in the King Swing traverse to a new crack system, on his 100th climb of The Nose, on El Capitan. The loose flake ('Boot Flake') relies on high φ.

Figure 20 c and d.

Figure 20 shows several examples of the widespread degradation of steep mountain-sides, at different scales. The 'flake' at the side of the Cerro Torre peak (Fig. 20c) is probably as long as 200m, and presumably started as a minor extension process, followed by the continuous effects of temperature cycling, water-pressure cycling,, ice-wedging, and successively 'more successful' block-fall wedging of the inner-surface of the now huge crack.

Figure 20d is an unusual action shot from the book by Florian and Moye, 2016 and shows one of the wider (body-wide) cracks which exists behind the loosened and partly fallen so-called 'Boot Flake' on the famous 'Nose' route up the 1,000m high El Capitan face in Yosemite. There is another even larger 'flake' down to the right side called the 'Texas Flake' signifying the relentless degradation. Elsewhere there are giant slabs.

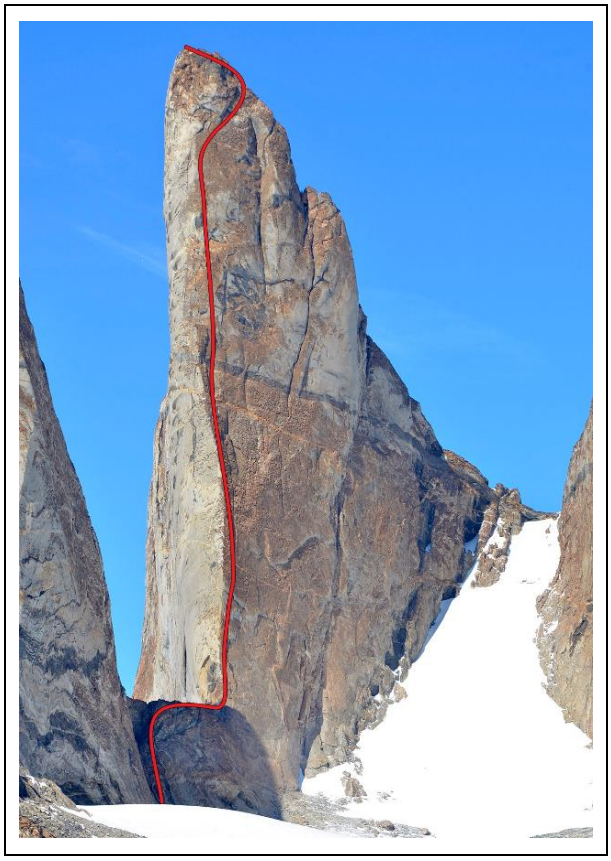

Figure 21. Bertha's Tower, 600m high, Wolthat Mountains (Droning Maud Land, Antarctica) located approximately 150 km *east* of the Fenris area around Ulvetanna, Possible more 'recent' left-face failure judging by colour change. Annotated (climbing route) photo from internet: AAJ Climbs and Expeditions, author/climber Mike Libecki, 2013. (The mountain was climbed in 2012).

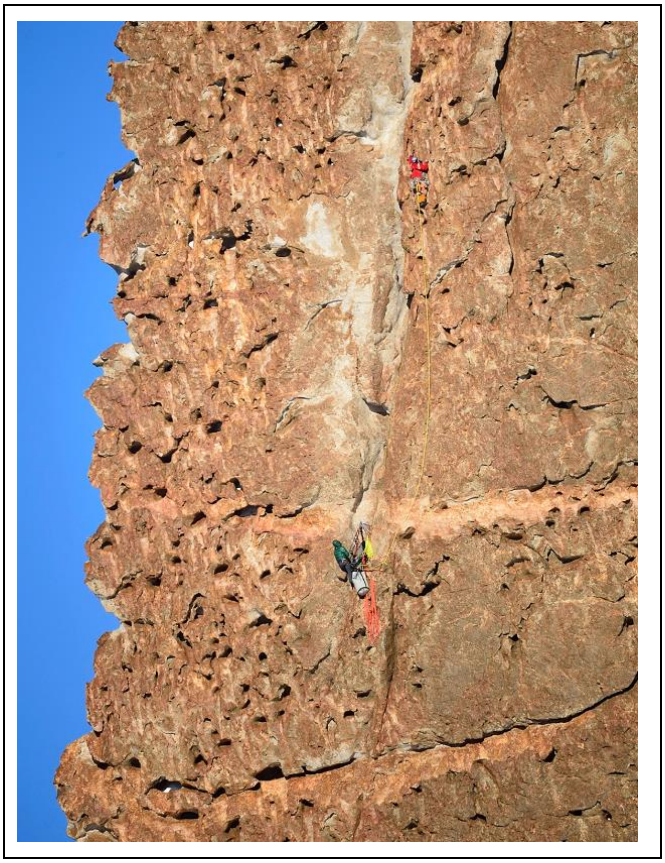

Figure 22. An interesting weathering-related description of part of the route marked in Figure 20. Quoting from Libecki's 2013 climbing description: *'It sometimes seemed we were on a skyscraper of petrified Swiss cheese. At one point I found myself climbing over an expanse of orange and white quartz crystals, using the jewels and gemstones for hand and foot holds.'* Relentless cold and very strong winds were experienced by the climbers.

In Antarctica there are some especially interesting features in the unique mountains. The brown/weathered mountain face seen in Figure 21 (detail in Figure 22) is perhaps demonstrating ancient shear failure surfaces, now with weathered, ice-wedged and eroded-wide apertures at 60° (oldest next to snow), 70° (also very ancient) and 80° (more 'recent' closest to present-day left-face). Theoretically (45° + φ/2) inclined ancient failure-planes, along directions of maximum shear stress from different geological eras (with a previously higher mountain), and non-linear stress-dependence of φ (as in Figure 12), would need φ to have been respectively 30°, 50° and 70°. Each are perfectly feasible when there is acceptance of non-linear critical-state based shear strength, rather than the actually impossible Mohr-Coulomb linearity (Barton, 1976, Singh et al. 2011). The description of the weathered 'Swiss cheese skyscraper' in Figure 22 emphasizes that for some reason (extreme dryness and high winds?) the extension-slab release mechanism is now only partly active on this ancient mountain wall (see flake, top-right). Another possible *macro-shear-mechanism* photo is shown in Figure 23. This is a dramatic example that shearing could occur.

Figure 23. Holtanna, a mostly massive 750m high monolith, in Dronning Maud's Land, Antarctica, shows a classically-inclined plane of maximum shear stress (perhaps even prior rotation?). The *apparently* tilted photo on the right is reproduced to emphasise the incipient failure plane more clearly, due to more revealing shadow. But the photo has been taken from a location perhaps 1km to the left of the skier, and views the 750m high tower from another angle. Perhaps there would be signs of pre-peak shear and dilation if the inclined plane could be examined by climbers with an *added* appreciation of rock mechanics. Climbers are already our chief observers, and avid users, of mountain degradation features.

Steph Davis, one of the world's foremost free-solo experts, on Zion N.P. sandstone. Note smoothness of the extensional fractures in the main face of the cliff wall.

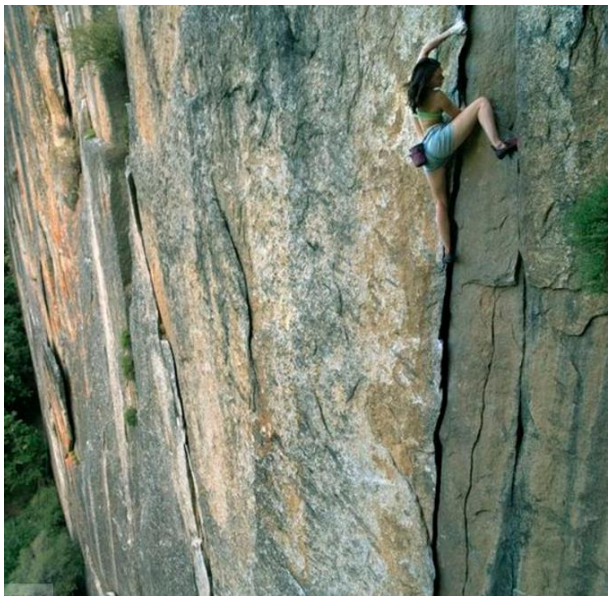

Steph Davis ('Learning to Fly') on the Outer Limits route of El Capitan, Yosemite N.P. Numerous exfoliation and extensional fractures are evident.

Figure 24 a and b.

Free-solo ace, Alex Honnold ('Alone on the Wall') testing himself on Thank God Ledge, Half Dome. The exfoliation process is very active in Yosemite.

Alex Honnold first free-soloist of Moonlight Butress in Zion N.P. sandstone. Long, smooth face fractures and long perpendicular fractures are typical.

Figure 24 c and d.

Rock climbers actually depend on the process of geomorphological degradation a) for the steepness of specific mountain walls in climbing mecca like Yosemite, Patagonia, Karakoram etc., (b) for their best holds, i.e. for the most continuous near-vertical crack systems. The extension-strain existence of the latter represents a huge contribution to the existence of commercial rock climbing gear, both for hobby and sports climbers, because *devices for wedging into cracks* exist in their thousands, and are sold in their millions. They are, for many, a necessity for safer climbing, and represent a welcome substitute for first and second finger-joints, fists, feet and whole bodies when behind loosened ('post-peak') flakes. Both the smooth, often continuous faces, and the long vertical cracks are the product, in effect, of vertical gravity-induced local 'tectonics'. They depend first on g, then tectonics, then H, γ, and ν, causing exceedence of critical extensional

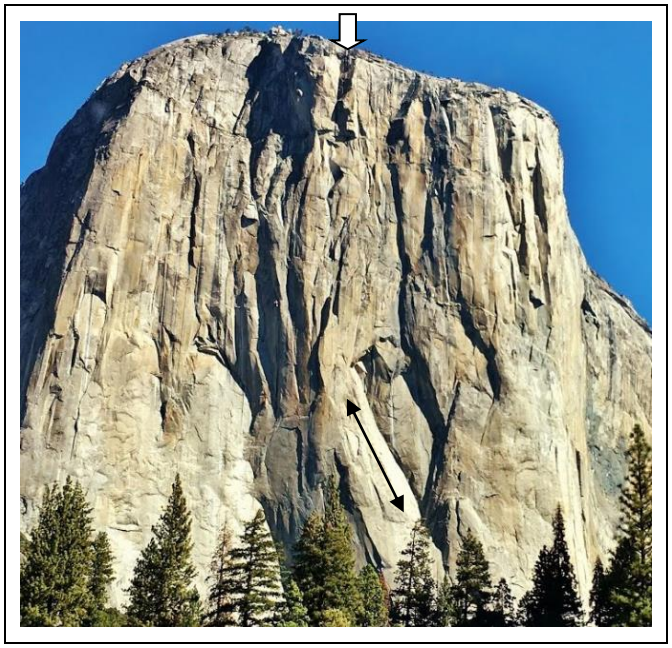

Figure 25 a and b. Two contrasting scales of potential failure of El Capitan. In the top photograph there is strong evidence of a major ≈ 400m long shear surface. Whether this is a 'classic' fore-runner to a large future rock avalanche may depend on the 'competing' process of frontal degradation of both plane and curved extension-failure surfaces, as depicted at close quarters in the lower figure.

strain ε_c , and finally the insufficient tensile strength σ_t. The latter is inexorably reduced over time by diurnal and seasonal temperature fluctuation, with rain and ice in turn, causing water pressures and ice-wedging.

8. FRACTURING AND JOINTING

Although the 'curved surface' origins of sheeting joints frequently proposed by Martel, 2017 are obviously valid mechanical arguments, it appears that the role of Poisson's ratio may not have been widely appreciated.

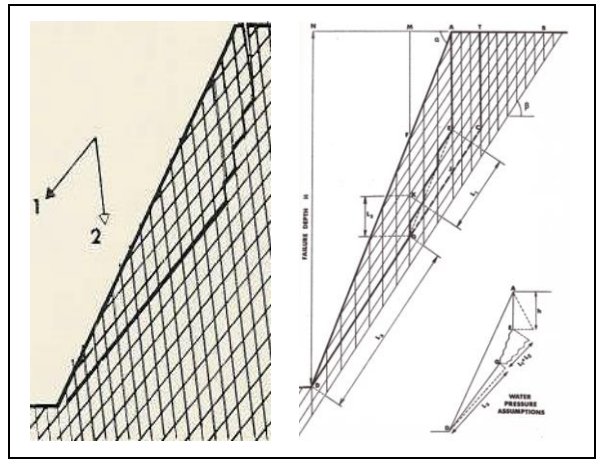

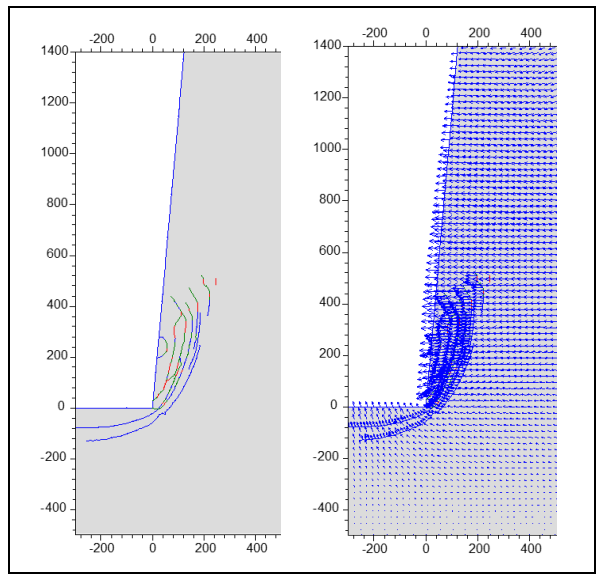

Figure 26. Top: A highly idealized, adversely jointed and progressively failing rock slope, which would eventually collapse along a stepped failure surface (Barton, 1971). Bottom: The potential failure of a high (1,400m) mountain wall in massive rock of insufficient uniaxial compressive strength (UCS = 60 MPa), modelled with FRACOD, with extensional fractures propagating in widespread shearing behind the highly stressed-and-therefore-strained toe. With the assumed density of 2.6 tons/m^3, an assumed tensile strength of only 5MPa, and Poisson's ratio of 0.25, equation 10 predicts H_c = 770m. (5 x 100)/(2.6 x 0.25): the 1,400m wall must fail.

There are many exfoliation/extensional features with quite planar or extremely planar origins: several are seen on the previous 'rock climbing page'. Holzhausen, 1989 documented that exfoliation/sheeting joints can occur at up to 10's of meters depth, though with a tendency for greatly increased spacing or decreased frequency beyond about 10-20m. Some 10 to 15m deep exfoliation joints can be seen in some parts of the walls of El Capitan, where prior slab falls have ocurred in the distant past and exposed their edges.

Figures 25 and 26 are deliberately shown in parallel because four mechanisms of rock slope degradation (and possible failure) are shown. The ≈ 400m long shear

surface seen as the lightest colour (white) in Figure 25a is evidence of a prior rock avalanche event (and a much larger one 'behind' it), with huge volumes of debris perhaps removed by later glaciation. How many millenia will have to pass before another, probably larger event occurs, even unthinkably taking some of the famous Nose, is dependent on many factors, not least the existence, or not, of a 'viable' vertical tension crack system.

In the deliberately jointed and deliberately unstable Figure 26a, which was produced during a 'steep excavated rock slope' study during Ph.D. thesis years with mining company (Rio Tinto) support (Barton, 1971), a down-stepped progressively shearing region was proposed, with the help of rather conservative 'triangular' water pressure assumptions (inset). It has slight similarity to the continuous feature in partial shadow, steeply stepped, and marked with a white arrow in Figure 25a. Hopefully and much more likely, the frontal degradaton loved by rock climbers (Figures 24 a and c, and 25 b) will continue for millennia, and 'pre-empt' the potential rock avalanche event, which at this potential scale are extremely rare.

The FRACOD fracture model shown in Figure 26b, is a deliberatly marginal case, firstly because of an assumed extreme almost-vertical height of 1,400m, and secondly because of insufficient long-term UCS of only 60 MPa, and a tensile strength of 5MPa. If a high mountain tower, like the Great Trango (Figure 17c) is modelled with these same parameters, and appropriate mode I and mode II fracture toughness, its life would be very short. Note that both FRACOD modelled cases show shearing inside the base, either somewhat curved, or more planar and in effect making a potential down-stepping, or plane surface if intact bridges get sheared through.

8. SHADOWS ON YOSEMITE'S EL CAPITAN

Further views of The Nose are seen in various side views (in Figure 27 a through e). The slices of black-and-white photographs have been chosen to 'throw light' on details concerning possible tension cracks, that can be seen both below (vertically) and above (in sub-vertical steps) in relation to the approximately 400m of the visible shear plane marked with a thin double-tipped arrow in Figure 25a. It is remarkable how different shadows can suggest different prior, and possible future mountain degradation events. Close study of Figure 26 suggests that there could be some 'connection' (a vertical tension crack) between the upper and lower major shear planes. These two sub-parallel and steeply dipping 400 to 600m long surfaces are seen in Figure 25a, and in Figures 27 c and d. However the Nose, if toe-covered sufficiently deeply by debris, may keep nearly-stable for countless millenia.

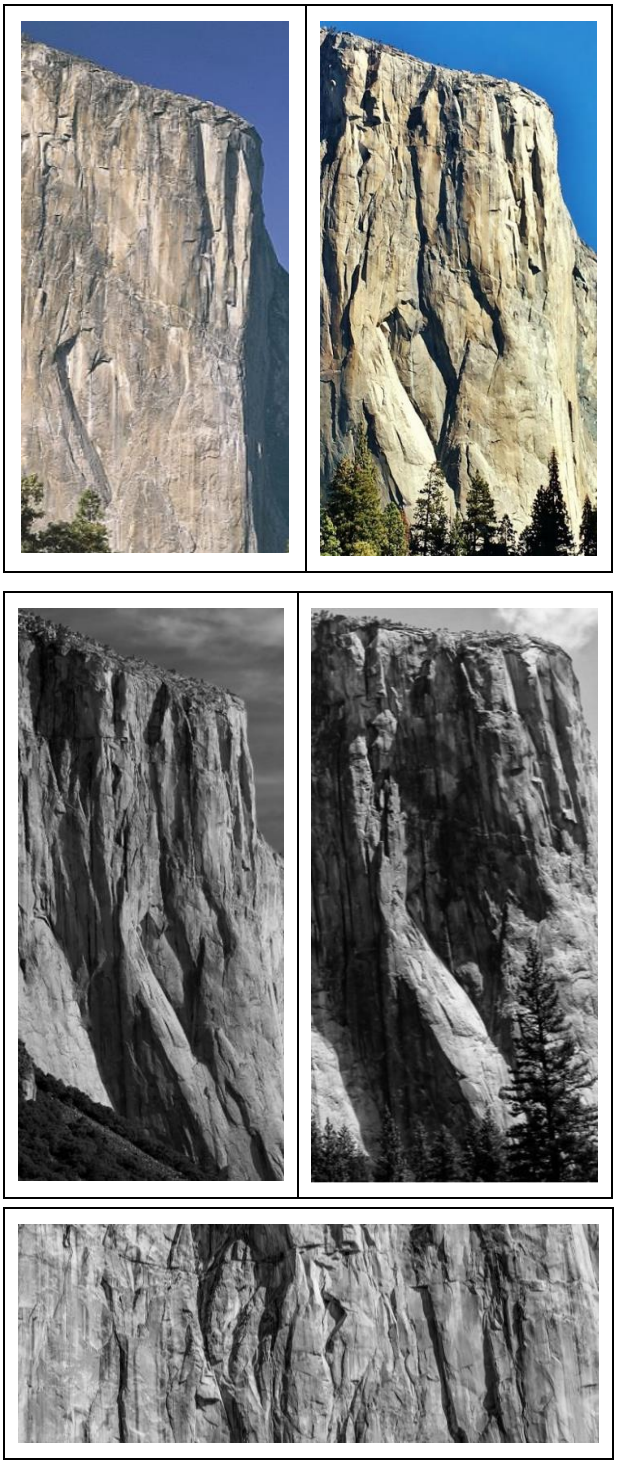

Figure 27. Different perspective from Figure 25c caused by absence or presence of different shadow angles. The 'small' triangular fall-out at ¾-height is in all photos. It is possibly as much as 50m high. The question remains. Has the long upper shear plane connection to higher-placed tension cracks? Have there been elongated slab-failures since Fig. 27a was taken?

9. THREE DEGRADATION PROCESSES

By a happy coincidence our interest in fracture development and propagation correspond with the four features that top rock climbers seem to value most: the steeper the better, the higher the better,

the smoother the better, the more semi-vertical cracks the better (or the means and skill to traverse to new crack systems). Of course the more cracks, the more a location like El Capitain is appreciated by a much wider climbing profession, provided the rock is strong like granite.

For the free-soloists, the existence of cracks behind developing slabs, and vertical cracks that are mostly as large as or larger than finger thicknesses is all part of their game, which includes negotiating detached slabs ('flakes'). For the semi-continuous subvertical cracks to be 'so wide' as say 20mm, massive mostly sparsely jointed conditions are needed. The parameter combination $\sigma_t/\gamma.\nu$ helps to generate many climbing features. Some are sketched in Figure 28 a, b and c. They all have to do with the slow degradation of the mountains. Numerous rock falls and some slab slides bear witness to this, as documented in Stock et al. 2012a.

Non-linear shear strength appreciation helps us to understand climbers apparent trust in high total friction angles (e.g. Figure 20d, the 'Boot Flake' on El Capitan 'The Nose'). We can possibly explain it's lack of further sliding (assuming no toe support) by the following equation, specifically when the normal stress is extremely low, and with effective JRC much reduced due to completely lost interlock.

$$\tau = \sigma_n' \tan [JRC \log_{10} (JCS/\sigma') + \varphi_r] \qquad (12)$$

where JRC = joint roughness coefficient (it varies from 0 if smooth-planar) to 20 (if extremely rough), JCS = joint wall compressive strength (it reduces with weathering) and φ_r = residual friction angle (also reduces with weathering). (See Barton, 2013 for further details).

The lower diagram (Figure 28 d) shows the gradual development of continuous deep tension cracks. If they occur there may be increased shear stress at the base (both are inter-dependent processes) and a certain degree-of-freedom for down-dip shearing might develop. Since we can have vertical stresses exceeding 25 MPa under such 1,000m high mountain walls, the possibility of minor shear displacement or even failure becomes real, and is seen as historic events in El Capitan photographs on the previous page. Figure 25a and Figure 27 a through d, also suggest this likely degradation of strength properties. Note the intended progression from shear resistance of τ_1 to τ_2 in Figure 28 d to e. In the huge time interval between the sketched events, JRC (joint roughness), JCS (joint wall strength) and φ_r (residual friction angle of a flat surface) are each likely to degrade significantly.

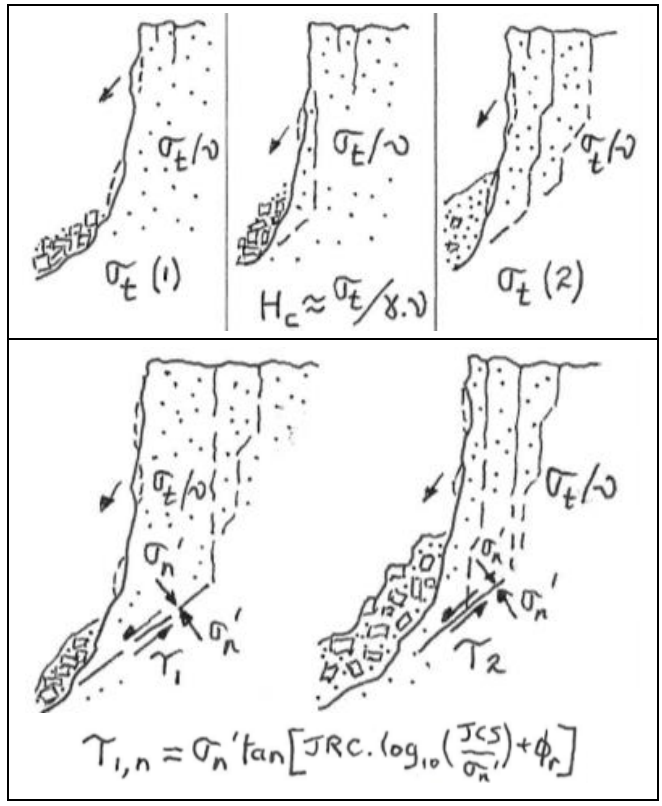

Figure 28 a through e. Sketches to illustrate ideas about the gradual degradation of steep mountain slopes in glaciated terrain. The upper three diagrams depict gradual degradation of the tensile strength from $\sigma_{t\,1}$ to $\sigma_{t\,2}$, and the consequences in terms of frontal falures from block falls, to slab slides, to possible large rock slides. Degrading shear *resistance* τ_1 and τ_2 is the dilemma, also due to eventual failure of rock 'bridges'.

CONCLUSIONS

1. Stress or strain induced fracturing in massive rock, when initially without the complications of fracturing or jointing, can benefit from the application of linear elastic theory. One of the irresistible processes, besides axial shortening caused by applying a principal stress, is the lateral expansion: the perpendicular Poisson effect which accompanies the shortening.

2. Taking a 1km deep tunnel in massive rock as an example, the maximum principal stress of maybe 50MPa is the newly generated tangential stress. Besides the reduction of the radial stress to zero at the tunnel periphery, there will be a Poisson's ratio expansion of the rock towards the newly created free surface of the tunnel. Radial deformation is registered, but it is actually caused by tangential strain, by Poisson's ratio, and by σ_r becoming almost zero (minus support pressure).

3. The tunnelling profession has previously utilized the ratio of the tangential stress in relation to the UCS of the intact rock to assess risk of fracturing. Numerous tunnels

in massive rock have demonstrated that when this ratio reaches 0.4±0.1, stress *(actually it is strain)* induced fracturing, also acoustic emission begins. At higher stress levels there may be rock bursting due to sudden propagation in shear, which is an unstable process.

4. In the Q-system of rock mass classification, which is used for helping select tunnel support, the stress reduction factor SRF is accelerated when reaching and going beyond this stress/strength ratio. In later Canadian tunnelling research, independently from SRF, the same ratio of σ_θ/UCS, when exceeding 0.4±0.1 is used to suggest depth of stress (*actually strain*) induced failure.

5. We now know from the presently reported research that the critical value of σ_θ (when fracturing begins) can more correctly be expressed as the ratio of tensile strength and Poisson's ratio (σ_t/ν). Initial fracturing is extension-strain controlled, with propagation in shear if depth and stress is high enough. This is proved by DDM (displacement discontinuity method) fracture mechanics modelling with FRACOD, with mode I *and* mode II defined fracturing, the latter unusual in modelling.

6. In the case of high mountain walls, which may have been (over-) steepened in the past by glacial processes, there is an apparent lack of understanding of how to predict major rock avalanches, and the more minor but frequent exfoliation slabbing. The Yosemite Valley is a perfect observational laboratory, with thousands of smaller slabbing and rock fall events, but few geologically recent major rock avalanches. Furthermore, there is a wealth of 'unintended' rock mechanics observation from rock climbing photos. Extensional fracturing, making finger-sized and larger cracks represent the climber's laborious routes to the top, and are in effect the main-stay of the commercial climbing gear companies. They have thousands of solutions for wedging in extension cracks of different sizes, and roping between the secure points.

7. It has been argued by others that a viable mechanism to explain the exfoliation slabbing and 'flakes' (as referred in climbing) is curvature and the generation of tensile stresses. Since a huge proportion of slabs and flakes are nevertheless planar, sometimes over very large areas measuring 100's of meters in both directions, and since cracks may sometimes continue upwards for hundreds of meters, another mechanism of origin for sheeting joints is needed, other than curvature. As in deep tunnels, the origin is *extension fracturing*, maybe with all three principal stresses compressive. Poisson's ratio is the frequent culprit, causing a critical tensile strain to be exceeded. Down a steep mountain face we can crudely equate the ratio σ_t/ν with an approximate principal stress, generated by height and density, and of course gravity.

8. As a result we have discovered that the critical height of a vertical cliff H_c can be roughly equated to $\sigma_t/\nu.\gamma$ where γ is the density in appropriate units. This simple equation can be used to explain the world-wide limit of 1,200 to 1,300m as the approximate range of the highest near-vertical mountain walls. The same equation can be used to predict failure of 10 to 20m high cliffs in the very weak Cappadocia tuffs, where tensile strength may be < 0.1MPa, compared to 5 to 10 MPa in the world's highest near-vertical mountain walls.

9. Soil mechanics related formulæ starting with Coulomb, and involving the over-coming of cohesive strength, with lowerbound and upperbound solutions depending on method of analysis: limit equilibrium or limit state, seriously over-estimate vertical cliff heights *in rock* by a factor or three to six times. This is because rock at large scale seldom fails like soil at much smaller scale. A uniaxial strength-based approximation suggested by Terzaghi, 1962 has equal difficulty, and Terzaghi immediately proposed the weakening effect of jointing to explain the gross over-estimation of his equation.

10. An interesting corollary to this same Terzaghi UCS/γ approximation is that with substitution of UCS for a strong rock like granite, one apparently obtains a non-vertical 'mountain height' limit of 7 to 8 km. However such application is flawed, and was not intended by Terzaghi either, although others have used this erroneous formulation when estimating why there are *only* fourteen mountains worldwide > 8,000m, and none reaching 9,000m.

11. The reality of the shear strength of intact (and jointed) rock is a strongly curved strength envelope all the way up to the critical state where higher strength is impossible. Mohr-Coulomb linearity cannot help here. Significantly, the maximum confined compressive strength may be three times higher than the uniaxial strength (Figure 12 needs to be referenced). The maximum possible shear strength at the critical state is of similar numerical magnitude to UCS, say 200 MPa for a strong rock like granite.

12. The *shear strength* at these high mountain-base depths of roughly 10 km (allowing for some isostatic depth adjustment) is the weakest link, far lower than the *confined compressive strength*.

13. In conclusion H_c for mountains is *shear-strength* controlled, while H_c for vertical cliffs is *tensile-strength* (and Poisson's ratio) controlled. These two strengths are the weakest links in *geology and geomorphology*.

REFERENCES

Aydan, Ö. And Ulusay, R. 2016. Rock engineering evaluation of antique rock structures in Cappadocia Region of Turkey.

Rock Mechanics and Rock Engineering: From the Past to the Future. Ulusay et al. (Eds), Taylor and Francis.

Addis, M.A., Barton, N., Bandis, S.C. & Henry, J.P. 1990. Laboratory studies on the stability of vertical and deviated boreholes. *65th Annual Technical Conference and Exhibition of the Society of Petroleum Engineers*, New Orleans, September 23-26, 1990.

Barton, N. 1971. *A model study of the behaviour of steep excavated rock slopes. Ph.D. Thesis*, Univ. of London.

Barton, N. & Grimstad, E. 1994. The Q-system following twenty years of application in NMT support selection. *43rd Geomech. Colloquy*, Salzburg. Felsbau, 6/94. pp. 428-436.

Barton, N. & Warren, C. 1996. Rock mass classification of chalk marl in the UK Channel Tunnels. *Channel Tunnel Engineering Geology Symp.*, Brighton, September 1995.

Barton. N. 2003. Failure around tunnels and boreholes and other problems in rock mechanics. *Letter to ISRM News Journal*, October, 12-18.

Barton, N. & Infanti, N. 2004. Unexpected stress problems in shallow basalts at the Ita hydroelectric power project in S.E. Brazil. *Proc. ARMS 2004 : 3rd Asian Rock Mechanics Symposium*, Kyoto.

Barton. N. 2010. Low Stress and High Stress Phenomena in Basalt Flows. Keynote paper. *3rd International Workshop on Rock Mechanics and Geo-Engineering in Volcanic Environments.* Tenerife.

Barton, N. 2013. Shear strength criteria for rock, rock joints, rockfill and rock masses: problems and some solutions. *J. of Rock Mech. & Geotech. Engr*., Wuhan, Elsevier 5(2013) 249-261.

Barton, N. & Grimstad, E., 2014. Q-system - an illustrated guide following forty years in tunnelling. *NB&A Web site www.nickbarton.com*, 43p.

Barton, N. and E. Quadros, 2015. Anisotropy is everywhere, to see, to measure and to model. *Rock Mechanics and Rock Engineering*, July 2015, Volume 48, 1323-1339.

Barton, N. and Shen, B., 2016. Risk of shear failure and extensional failure around over-stressed excavations in brittle rock. Keynote lecture, Geosafe 2016. *1st. Int. Symp. on Reducing Risks in Site Investigation, Modelling and Construction for Rock Engineering.* Xi'an, China. http://dx.doi.org/10.1016/ j.jrmge.2016.11.004. Publ. in J. of Rock Mech. & Geotech. Eng., Elsevier.

Barton, N. 2016. Cavern and Tunnel Failures due to Adverse Structural Geology. *2nd International Specialized. Conf. on Soft Rocks*, Cartagena, Colombia. Keynote lecture. 18p.

Bray, J.W. 1967. A study of jointed and fractured rock. Part I. Fracture patterns and their failure characteristics. *Felsmechanik, V/2-3, 117-136.*

Chen, W.F. and C.R. Scawthorn, 1968. Limit analysis and limit equilibrium analyses in soil mechanics. *FEL, Lehigh Univ.* Pennsylvania.

Davis, S. 2013. *Learning to Fly: An Uncommon Memoir of Human Flight, Unexpected Love, and One Amazing Dog.* A Touchstone Book, Simon & Schuster, New York, 292p.

Drucker, D.C. and W. Prager,1952. Soil mechanics and plastic analysis or limit design. *Quarterly Applied Mathematics*, 10, 157-165.

Florine, H. and J. Moye, 2016. *On the Nose – A lifelong obsession with Yosemite's most iconic climb.* Rowman & Littlefield/ Falcon & National Book Network. 203p.

Grimstad, E. & Barton, N. 1993. Updating of the Q-System for NMT. *Proc. of the Int. Symp. on Sprayed Concrete –*

Modern Use of Wet Mix Sprayed Concrete for Underground Support, Fagernes, 1993, Eds Kompen, Opsahl and Berg. Norwegian Concrete Association, Oslo, 46-66.

Heyman, J. 1973. The stability of a vertical cut. *Int. J. of Mech. Sciences*, 15(10): 845-854.

Holzhausen, G.R. 1989. Origin of sheet structure. 1. Morphology and boundary conditions. *Engineering Geology* 27: 225-278.

Honnold, A. and D. Roberts, 2016. *Alone on the Wall.* W.W. Norton & Company, New York. 248p.

Howard, A.D. and M.J. Selby, 1994. Rock slopes. *Geomorphology of Desert Environments*. Eds. Abrahams and Parsons, Chapman & Hall, London.

Kaşmer, Ö, Ulusay, R. and Geniş, M., 2013. Assessments on the stability of natural slopes prone to toe erosion, and man-made historical semi-underground openings carved in soft tuffs at Zelve Open-Air Museum (Cappadocia, Turkey). *Engineering Geology* 158 (2013) 135-158.

Martel, S.J. 2017. Progress in understanding sheeting joints over the past two centuries. *Jour. of Structural Geology*, Elsevier, 94, 68-86.

Martin, C.D., Kaiser, P.K. & McCreath, D.R. 1998. Hoek–Brown parameters for predicting the depth of brittle failure around tunnels. *Can. Geotech. J.* 36, 136-151.

Melosh, H.J. 2011. *Planetary Surface Processes*. Cambridge University Press, Cambridge, UK.

Shen, B., Stephansson, O. & Rinne, M., 2013. *Modelling Rock Fracturing Processes: A Fracture Mechanics Approach Using FRACOD.* Springer, 173p.

Singh, M., Raj, A. and B. Singh. Modified Mohr-Coulomb criterion for non-linear triaxial and polyaxial strength of intact rocks. 2011. *I J. Rock Mech. Min. Sci.*, 48(4), 546-555.

Siren, T. 2012. Fracture Toughness Properties of Rocks in Olkiluoto: Laboratory Measurements 2008–2009, *Posiva Report* 2012-25.

Stacey, T.R. 1981. A simple Extension Strain Criterion for Fracture of Brittle Rock. *Int. J. Rock Mech. Min. Sci. & Geomech. Abstr.* 18, 469-474.

Stock, G.M., N. Luco, B.D. Collins, E.L. Harp, P. Reichenbach, and K.L. Frankel, 2012. Quantitative rock-fall hazard and risk assessment for Yosemite Valley, *Yosemite National Park*, California. USGS.

Terzaghi, K. 1962. Stability of steep slopes on hard unweathered rock. *Geotechnique* 12: 251-263.

Verruijt, A. 2001. *Soil Mechanics.* Delft University of Technology, The Netherlands.

Weber, S., J. Beutel, J. Faillettaz, A. Hasler, M. Krautblatter and A. Vieli. 2016. Quantifying irreversible movement in steep fractured bedrock permafrost at Matterhorn (CH). *The Cryosphere Discussions Journal. (in press).*

Wolters, G. and G. Müller, 2008. Effect of cliff shape on internal stresses and rock slope stability. *J. of Coastal Research*, 24(1), 43-50, Florida.